

DIRAC/PS212

CERN-PH-EP-2016-128
May 20, 2016

Observation of $\pi^- K^+$ and $\pi^+ K^-$ atoms

B. Adeva¹⁾, L. Afanasyev²⁾, Y. Allkofer³⁾, C. Amsler⁴⁾, A. Anania⁵⁾, S. Aogaki⁶⁾, A. Benelli⁷⁾,
V. Brekhovskikh⁸⁾, T. Cechak⁷⁾, M. Chiba⁹⁾, P. Chliapnikov⁸⁾, P. Doskarova⁷⁾, D. Drijard¹⁰⁾,
A. Dudarev²⁾, D. Dumitriu⁶⁾, D. Fluerasu⁶⁾, A. Gorin⁸⁾, O. Gorchakov²⁾, K. Griksay²⁾, C. Guaraldo¹¹⁾,
M. Gugiu⁶⁾, M. Hansroul¹⁰⁾, Z. Hons¹²⁾, S. Horikawa³⁾, Y. Iwashita¹³⁾, V. Karpukhin²⁾, J. Kluson⁷⁾,
M. Kobayashi¹⁴⁾, V. Kruglov²⁾, L. Kruglova²⁾, A. Kulikov²⁾, E. Kulish²⁾, A. Kuptsov²⁾, A. Lamberto⁵⁾,
A. Lanaro¹⁵⁾, R. Lednicky¹⁶⁾, C. Mariñas¹⁾, J. Martincik⁷⁾, L. Nemenov^{2,10)}, M. Nikitin²⁾, K. Okada¹⁷⁾,
V. Olchevskii²⁾, M. Pentic⁶⁾, A. Penzo¹⁸⁾, M. Plo¹⁾, P. Prusa⁷⁾, G. Rappazzo⁵⁾, A. Romero Vidal¹¹⁾,
A. Ryazantsev⁸⁾, V. Rykalin⁸⁾, J. Saborido¹⁾, J. Schacher^{4,*)}, A. Sidorov⁸⁾, J. Smolik⁷⁾, F. Takeuchi¹⁷⁾,
L. Tauscher¹⁹⁾, T. Trojek⁷⁾, S. Trusov²⁰⁾, T. Urban⁷⁾, T. Vrba⁷⁾, V. Yazkov²⁰⁾, Y. Yoshimura¹⁴⁾,
M. Zhabitsky²⁾, P. Zrelov²⁾

DIRAC Collaboration

¹⁾ Santiago de Compostela University, Spain

²⁾ JINR, Dubna, Russia

³⁾ Zurich University, Switzerland

⁴⁾ Albert Einstein Center for Fundamental Physics, Laboratory of High Energy Physics, Bern, Switzerland

⁵⁾ INFN, Sezione di Trieste and Messina University, Messina, Italy

⁶⁾ IFIN-HH, National Institute for Physics and Nuclear Engineering, Bucharest, Romania

⁷⁾ Czech Technical University in Prague, Czech Republic

⁸⁾ IHEP, Protvino, Russia

⁹⁾ Tokyo Metropolitan University, Japan

¹⁰⁾ CERN, Geneva, Switzerland

¹¹⁾ INFN, Laboratori Nazionali di Frascati, Frascati, Italy

¹²⁾ Nuclear Physics Institute ASCR, Rez, Czech Republic

¹³⁾ Kyoto University, Kyoto, Japan

¹⁴⁾ KEK, Tsukuba, Japan

¹⁵⁾ University of Wisconsin, Madison, USA

¹⁶⁾ Institute of Physics ASCR, Prague, Czech Republic

¹⁷⁾ Kyoto Sangyo University, Kyoto, Japan

¹⁸⁾ INFN, Sezione di Trieste, Trieste, Italy

¹⁹⁾ Basel University, Switzerland

²⁰⁾ Skobeltsin Institute for Nuclear Physics of Moscow State University, Moscow, Russia

* Corresponding author

Abstract

The observation of hydrogen-like πK atoms, consisting of $\pi^- K^+$ or $\pi^+ K^-$ mesons, is presented. The atoms have been produced by 24 GeV/ c protons from the CERN PS accelerator, interacting with platinum or nickel foil targets. The breakup (ionisation) of πK atoms in the same targets yields characteristic πK pairs, called “atomic pairs”, with small relative momenta in the pair centre-of-mass system. The upgraded DIRAC experiment has observed 349 ± 62 such atomic πK pairs, corresponding to a signal of 5.6 standard deviations.

1 Introduction

Up to now, the DIRAC collaboration has published indications about the production of πK atoms¹ [1–3]. This time, DIRAC reports the first statistically significant observation of the strange dimesonic πK atom.

Meson-meson interactions at low energy are the simplest hadron-hadron processes and allow to test low-energy QCD, specifically Chiral Perturbation Theory (ChPT) [4–7]. The observation and lifetime measurement of $\pi^+ \pi^-$ atoms (pionium) have been reported in [8–10]. Going one step further, the observation and lifetime measurement of the πK atom involving strangeness provides a direct determination of a basic S-wave πK scattering length difference [11]. This atom is an electromagnetically bound πK state with a Bohr radius of $a_B = 249$ fm and a ground state binding energy of $E_B = 2.9$ keV. It decays predominantly by strong interaction into two neutral mesons $\pi^0 K^0$ or $\pi^0 \bar{K}^0$. The atom decay width $\Gamma_{\pi K}$ in the ground state (1S) is given by the relation [11, 12]: $\Gamma_{\pi K} = \frac{1}{\tau} = R(a_0^-)^2$, where $a_0^- = \frac{1}{3}(a_{1/2} - a_{3/2})$ is the S-wave isospin-odd πK scattering length (a_I is the πK scattering length for isospin I) and R a precisely known factor (relative precision 2%). The scattering length a_0^- has been studied in ChPT [13–15], in the dispersive framework [16] and in lattice QCD (see e.g. [17]). Using a_0^- from [16], one predicts for the πK atom lifetime $\tau = (3.5 \pm 0.4) \cdot 10^{-15}$ s.

A method to produce and observe hadronic atoms has been developed [18]. In the DIRAC experiment, relativistic dimesonic bound states, formed by Coulomb final state interaction (FSI), are moving inside the target and can break up. Particle pairs from breakup (atomic pair in Fig. 1) are characterised by a small relative momentum $Q < 3$ MeV/c in the centre-of-mass (c.m.) system of the pair².

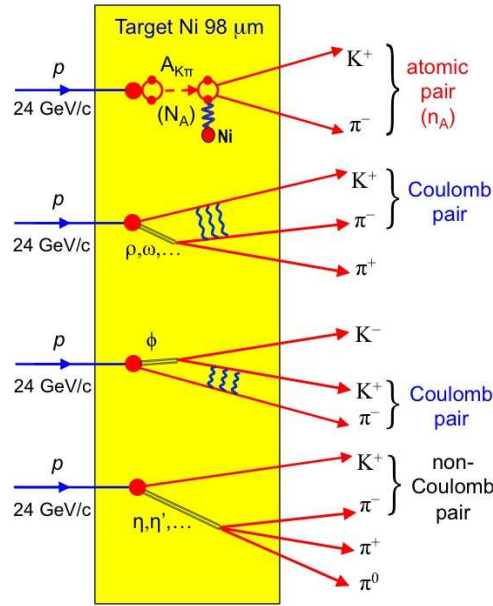


Fig. 1: Inclusive πK production in 24 GeV/c p-Ni interaction: $p + \text{Ni} \rightarrow \pi^- K^+ + X$. The ionisation or breakup of $A_{K\pi}$ leads to so-called atomic pairs. (More details, see text in section 3.)

A first πK atom investigation has been performed with a platinum target at the CERN PS with 24 GeV/c protons in 2007 [1, 2]. An enhancement of πK pairs at low relative momentum has been observed, corresponding to 173 ± 54 πK atomic pairs or a significance of 3.2 standard deviations (σ). In the

¹The term πK atom or $A_{K\pi}$ refer to $\pi^- K^+$ and $\pi^+ K^-$ atoms.

² The quantity Q denotes the experimental c.m. relative momentum. The longitudinal (Q_L) and transverse ($Q_T = \sqrt{Q_X^2 + Q_Y^2}$) components of the vector \vec{Q} are defined with respect to the direction of the total laboratory pair momentum.

experiment from 2008 to 2010, DIRAC has detected in a Ni target an excess of $178 \pm 49 \pi K$ pairs, an effect of only 3.6σ [3].

In the present paper, experimental data obtained in Ni and Pt targets have been analysed, using recorded informations from all detectors (see Fig. 2) and enhanced background description based on Monte Carlo (MC) simulations. Setup geometry correction, detector response simulation, background suppression and admixture evaluation have been significantly improved for all runs.

The above mentioned improvements allow a statistically reliable observation of πK atoms.

2 Experimental setup

The setup [19], sketched in Fig. 2, detects and identifies $\pi^+\pi^-$, π^-K^+ and π^+K^- pairs with small Q . The structure of these pairs after the magnet is approximately symmetric for $\pi^+\pi^-$ and asymmetric for πK . Originating from a bound system, these particles travel with the nearly same velocity, and hence for πK atomic pairs, the kaon momentum is by a factor of about $\frac{M_K}{M_\pi} \approx 3.5$ larger than the pion momentum (M_K is the charged kaon mass and M_π the charged π mass). The 2-arm vacuum magnetic spectrometer presented is optimized for simultaneous detection of these pairs [20, 21].

The 24 GeV/c primary proton beam, extracted from the CERN PS, hits a $(26 \pm 1) \mu\text{m}$ thick Pt target in 2007³ and Ni targets with thicknesses $(98 \pm 1) \mu\text{m}$ in 2008 and $(108 \pm 1) \mu\text{m}$ in 2009 and 2010⁴. The radiation thickness of the 98 (108) μm Ni target amounts to about $7 \cdot 10^{-3} X_0$ (radiation length).

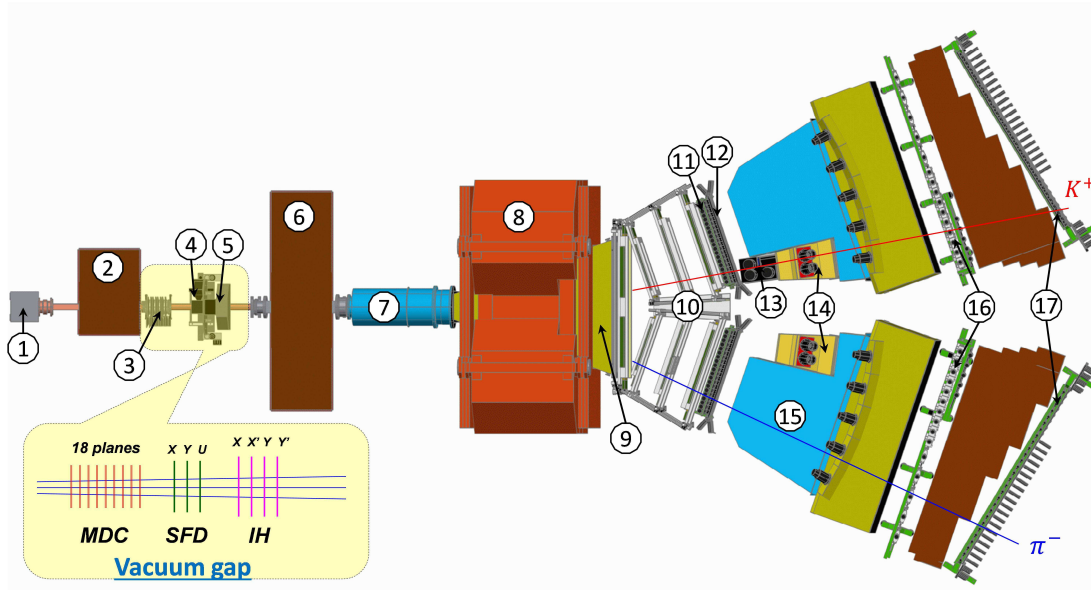


Fig. 2: General view of the DIRAC setup: 1 – target station; 2 – first shielding wall; 3 – microdrift chambers; 4 – scintillating fiber detector; 5 – ionisation hodoscope; 6 – second shielding wall; 7 – vacuum tube; 8 – spectrometer magnet; 9 – vacuum chamber; 10 – drift chambers; 11 – vertical hodoscope; 12 – horizontal hodoscope; 13 – aerogel Cherenkov; 14 – heavy gas Cherenkov; 15 – nitrogen Cherenkov; 16 – preshower; 17 – muon detector.

The secondary channel (solid angle $\Omega = 1.2 \cdot 10^{-3} \text{ sr}$) together with the whole setup is vertically inclined relative to the proton beam by 5.7° upward. Secondary particles are confined by the rectangular beam collimator inside of the second steel shielding wall, and the angular divergence in the horizontal (X) and

³ The Pt target maximizes production of atomic pairs.

⁴ The Ni targets are optimal for lifetime measurement.

vertical (Y) planes is $\pm 1^\circ$. With a spill duration of 450 ms, the beam intensity has been $(10.5\text{--}12) \cdot 10^{10}$ protons/spill and, correspondingly, the single counting rate in one plane of the ionisation hodoscope (IH) $(5\text{--}6) \cdot 10^6$ particles/spill. Secondary particles propagate mainly in vacuum up to the Al foil at the exit of the vacuum chamber, which is located between the poles of the dipole magnet ($B_{max} = 1.65$ T and $BL = 2.2$ T·m). In the vacuum gap, MicroDrift Chambers (MDC) with 18 planes and a Scintillating Fiber Detector (SFD) with 3 planes X, Y and U, inclined by 45° , have been installed to measure particle coordinates ($\sigma_{SFDx} = \sigma_{SFDy} = 60 \mu\text{m}$, $\sigma_{SFDu} = 120 \mu\text{m}$) and particle time ($\sigma_{tSFDx} = 380$ ps, $\sigma_{tSFDy} = \sigma_{tSFDu} = 520$ ps). The four IH planes serve to identify unresolved double track events with only one hit in SFD.

Each spectrometer arm is equipped with the following subdetectors: drift chambers (DC) to measure particle coordinates with about $85 \mu\text{m}$ precision; vertical hodoscope (VH) to measure time with 110 ps accuracy for particle identification via time-of-flight determination; horizontal hodoscope (HH) to select pairs with vertical separation less than 75 mm between the arms (Q_Y less than 15 MeV/c); aerogel Cherenkov counter (ChA) to distinguish kaons from protons; heavy gas (C_4F_{10}) Cherenkov counter (ChF) to distinguish pions from kaons; nitrogen Cherenkov (ChN) and preshower (PSh) detector to identify e^+e^- pairs; iron absorber and two-layer scintillation counter (Mu) to identify muons. In the “negative” arm, an aerogel counter has not been installed, because the number of antiprotons is small compared to K^- .

Pairs of oppositely charged time-correlated particles (prompt pairs) and accidentals in the time interval ± 20 ns are selected by requiring a 2-arm coincidence (ChN in anticoincidence) with a coplanarity restriction (HH) in the first-level trigger. The second-level trigger selects events with at least one track in each arm by exploiting DC-wire information (track finder). Using track information, the online trigger selects $\pi\pi$ and πK pairs with relative momenta $|Q_X| < 12$ MeV/c and $|Q_L| < 30$ MeV/c. The trigger efficiency is about 98% for pairs with $|Q_X| < 6$ MeV/c, $|Q_Y| < 4$ MeV/c and $|Q_L| < 28$ MeV/c. Particle pairs $\pi^- p$ ($\pi^+ \bar{p}$) from Λ ($\bar{\Lambda}$) decay have been used for spectrometer calibration and e^+e^- pairs for general detector calibration.

3 Production of bound and free $\pi^- K^+$ and $\pi^+ K^-$ pairs

Prompt $\pi^\mp K^\pm$ pairs from proton-nucleus collisions are produced either directly or originate from short-lived (e.g. Δ , ρ), medium-lived (e.g. ω , ϕ) or long-lived (e.g. η' , η) sources. Pion-kaon pairs produced directly, from short- or medium-lived sources, undergo Coulomb FSI resulting in unbound states (Coulomb pair in Fig. 1) or forming bound states ($A_{K\pi}$ in Fig. 1). Pairs from long-lived sources are practically not affected by Coulomb interaction (non-Coulomb pair in Fig. 1). The accidental pairs are generated via different proton-nucleus interactions.

The cross-section of πK atom production is given by the expression [18]:

$$\frac{d\sigma_A^n}{d\vec{p}_A} = (2\pi)^3 \frac{E_A}{M_A} \frac{d^2\sigma_s^0}{d\vec{p}_K d\vec{p}_\pi} \bigg|_{\frac{\vec{p}_K}{M_K} \approx \frac{\vec{p}_\pi}{M_\pi}} \cdot |\psi_n(0)|^2, \quad (1)$$

where \vec{p}_A , E_A and M_A are the momentum, total energy and mass of the πK atom in the laboratory (lab) system, respectively, and \vec{p}_K and \vec{p}_π the momenta of the charged kaon and pion with equal velocities. Therefore, these momenta obey in good approximation the relations $\vec{p}_K = \frac{M_K}{M_A} \vec{p}_A$ and $\vec{p}_\pi = \frac{M_\pi}{M_A} \vec{p}_A$. The inclusive production cross-section of πK pairs from short-lived sources without FSI is denoted by σ_s^0 , and $\psi_n(0)$ is the S -state Coulomb atom wave function at the origin with principal quantum number n . According to (1), πK atoms are only produced in S -states with probabilities $W_n = \frac{W_1}{n^3}$: $W_1 = 83.2\%$, $W_2 = 10.4\%$, $W_3 = 3.1\%$, $W_{n>3} = 3.3\%$.

In complete analogy, the $\pi^\mp K^\pm$ Coulomb pair production is described in the point-like production ap-

proximation, depending on the relative momentum q in the production point⁵:

$$\frac{d^2\sigma_C}{d\vec{p}_K d\vec{p}_\pi} = \frac{d^2\sigma_s^0}{d\vec{p}_K d\vec{p}_\pi} A_C(q) \quad \text{with} \quad A_C(q) = \frac{4\pi\mu\alpha/q}{1 - \exp(-4\pi\mu\alpha/q)}. \quad (2)$$

The Coulomb enhancement function $A_C(q)$ is the well-known Sommerfeld-Gamov-Sakharov factor [22–24], $\mu = 109 \text{ MeV}/c^2$ the reduced mass of the $\pi^\pm K^\pm$ system and α the fine structure constant. The relative production yield of atoms to Coulomb pairs [25] is calculated from the ratio (1) to (2).

For π and K production from non-pointlike medium-lived sources, corrections at the percent level have been applied to the production cross-sections [26]. Strong final state elastic and inelastic interactions are negligible [26].

4 Data processing

Recorded events have been reconstructed with the DIRAC $\pi\pi$ analysis software (ARIANE) modified for analysing πK data.

4.1 Tracking and setup tuning

Only events with one or two particle tracks in the DC detector of each arm are processed. Event reconstruction is performed according to the following steps:

- 1) One or two hadron tracks are identified in the DC of each arm with hits in VH, HH and PSh slabs and no signal in ChN and Mu (Fig. 2 and related text). The earliest track in each arm is used for further analysis, because these tracks induce the trigger signal starting the readout procedure.
- 2) Track segments, reconstructed in DC, are extrapolated backward to the incident proton beam position in the target, using the transfer function of the DIRAC dipole magnet. This procedure provides approximate particle momenta and corresponding intersection points in MDC, SFD and IH.
- 3) Hits are searched for around the expected SFD coordinates in the region $\pm 1 \text{ cm}$, corresponding to $3\text{--}5\sigma$ defined by the position accuracy, taking into account particle momenta. This way, events are selected with low and medium background defined by the following criteria: the number of hits around the two tracks is ≤ 4 in each SFD plane and ≤ 9 in all three SFD planes. The case of only one hit in the region $\pm 1 \text{ cm}$ can occur because of detector inefficiency (two crossing particles, but one is not detected) or if two particles cross the same SFD column. The latter event type can be regained by double ionisation selection in the corresponding slab of the IH. For data collected in 2007 with the Pt target, criteria are different: the number of hits is two in the Y - and U -plane (SFD X -plane and IH, which may resolve crossing of only one SFD column by two particles, have not been used in 2007). The momentum of the positively or negatively charged particle is refined to match the X -coordinates of the tracks in DC as well as the SFD hits in the X - or U -plane, depending on presence of hits. In order to find the best two-track combination, the two tracks may not use a common SFD hit in case of more than one hit in the proper region. In the final analysis, the combination with the best χ^2 in the other SFD planes is kept.

In order to improve the mechanical alignment and general description of the setup geometry, the Λ and $\bar{\Lambda}$ particle decays into $p\pi^-$ and $\pi^+\bar{p}$ are exploited [27–29]. By requiring the mass equality $M_\Lambda^{\text{exp}} = M_{\bar{\Lambda}}^{\text{exp}}$, the angles of the DC axes are modified. In the next step, the obtained angle between the DC axes is tuned to get the PDG (Particle Data group) reference Λ mass: the survey value of this angle needs to be increased by a few 10^{-4} rad. For the data set 2007–2010, the weighted average of the experimental Λ mass values is $M_\Lambda^{\text{exp}} = (1.115680 \pm 2.9 \cdot 10^{-6}) \text{ GeV}/c^2$, in agreement with the PDG value $M_\Lambda^{\text{PDG}} = (1.115683 \pm 6 \cdot 10^{-6}) \text{ GeV}/c^2$ [30]. This confirms consistency of the setup alignment. The Λ mass width in the simulated distribution tests how well the MC simulation reproduces the momentum and angle resolution of the setup. Data of each year has been investigated which simulated distribution – with different widths –

⁵ The quantity q denotes the original c.m. relative momentum.

fits best the experimental Λ distribution. Simulated Λ distributions providing a better χ^2 fit to the data are created with a width increased by the following factors: 1.027 ± 0.003 in 2007 (two SFD planes), while this increase in the subsequent years (three SFD planes) is not significant: 1.002 ± 0.004 (2008), 1.001 ± 0.003 (2009) and 1.003 ± 0.003 (2010). The difference between data and MC width could be the consequence of an imperfect description of the setup downstream part and can be removed by introducing a Gaussian smearing of the reconstructed momenta [3]. This technique is also used to evaluate the systematic error connected with reconstructed momentum smearing. Taking into account momentum smearing, the momentum resolution has been evaluated as $\frac{dp}{p} = \frac{p_{gen} - p_{rec}}{p_{gen}}$ with p_{gen} and p_{rec} the generated and reconstructed momenta, respectively. Between 1.5 and 8 GeV/c, particle momenta are reconstructed with a relative precision from $2.8 \cdot 10^{-3}$ to $4.4 \cdot 10^{-3}$ [27]. Relative momentum resolutions after the target are: $\sigma_{QX} \approx \sigma_{QY} \approx 0.36$ MeV/c, $\sigma_{QL} \approx 0.94$ MeV/c for $p_{\pi K} = p_{\pi} + p_K = 5$ GeV/c and about 6% worse values for $p_{\pi K} = 7.5$ GeV/c.

4.2 Event selection

Selected events are classified into three categories: $\pi^- K^+$, $\pi^+ K^-$ and $\pi^- \pi^+$. The last category is used for calibration purposes. Pairs of πK are cleaned of $\pi^- \pi^+$ and $\pi^- p$ background by the Cherenkov counters ChF and ChA. In the momentum range from 3.8 to 7 GeV/c, pions are detected by ChF with (95–97)% efficiency [31], whereas kaons and protons (antiprotons) do not produce a signal. The admixture of $\pi^- p$ pairs is suppressed by the aerogel Cherenkov detector (ChA), which records kaons but not protons [32]. By requiring a signal in ChA and selecting compatible time-of-flights (TOF) between the target and VH, $\pi^- p$ and $\pi^- \pi^+$ pairs, contaminating $\pi^- K^+$, can be substantially suppressed. Correspondingly, the admixture of $\pi^+ \pi^-$ pairs to $\pi^+ K^-$ has also been taken into account. Fig. 3 shows, after applying the selection criteria, the well-defined $\pi^- K^+$ Coulomb peak at $Q_L = 0$ and the strongly suppressed peak from Λ decays at $Q_L = -30$ MeV/c. The Q_L distribution of $\pi^+ K^-$ pairs is similar [3].

The final analysis sample contains only events which fulfil the following criteria:

$$Q_T < 4 \text{ MeV/c}, |Q_L| < 20 \text{ MeV/c}. \quad (3)$$

Due to finite detector efficiency, a certain admixture of misidentified pairs still remains in the experimental distributions. Their contribution has been estimated by TOF investigation and accordingly been subtracted [33]. Under the assumption that all positively charged particles are K^+ , Fig. 4 compares the experimental with the simulated TOF difference distribution for $\pi^- K^+$, $\pi^- \pi^+$ and $\pi^- p$ pairs. Two ranges for positively charged particle momenta, (4.4–4.5) and (5.4–5.5) GeV/c, have been investigated.

5 Data simulation

Since the πK data samples consist of Coulomb, non-Coulomb and atomic pairs, these event types have been generated by MC (DIPGEN [34], GEANT-DIRAC (setup simulator)). The MC sample exceeds ten times the number of experimental events. The events are characterised by different q distributions: the non-Coulomb pairs are distributed in accordance with phase space, while the q distribution of Coulomb pairs is modified by the factor $A_C(q)$ (2). For atomic pairs, one needs to know the breakup position and the lab momentum of each pair. In practice, lab momenta for MC events are generated in accordance with analytic formulae, resembling the experimental momentum distributions of such pairs [34, 35]. After comparing experimental momentum spectra [33] with MC distributions reconstructed by the analysis software, their ratio is used as event-by-event weight function for MC events in order to provide the same lab momentum spectra for simulated as for experimental data. The breakup point, from which the ionisation occurred, the quantum numbers of the atomic state and the corresponding q distribution of the atomic pair are obtained by solving numerically transport equations [36] using total and transition cross-sections [37]. The lab momenta of the atoms are assumed, in accordance with equation (1), to be

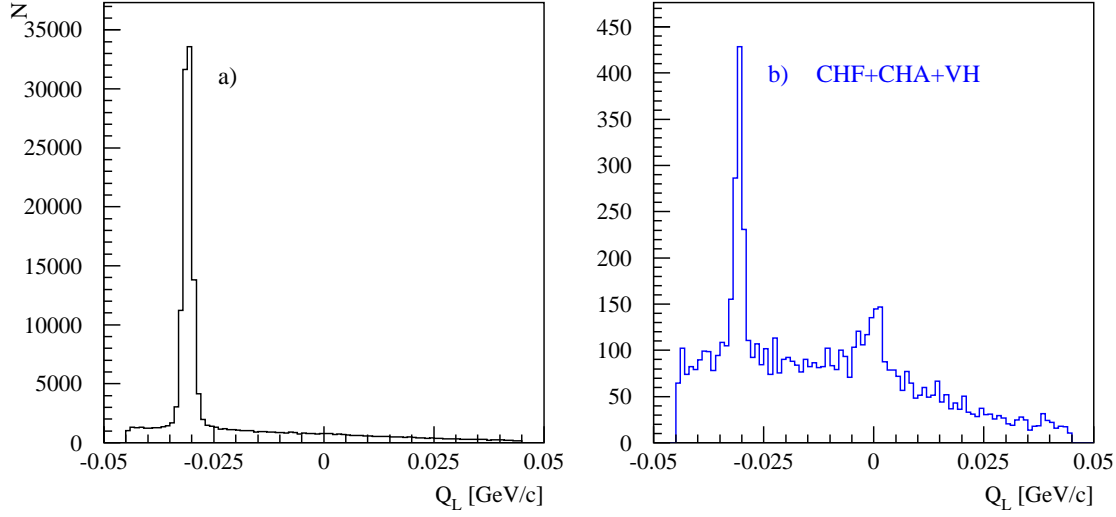


Fig. 3: Q_L distributions of potential $\pi^- K^+$ pairs before (a) and after (b) applying the selection described in the text. Events with positive Q_L are suppressed compared to those with negative Q_L due to lower acceptance and lower production cross-section.

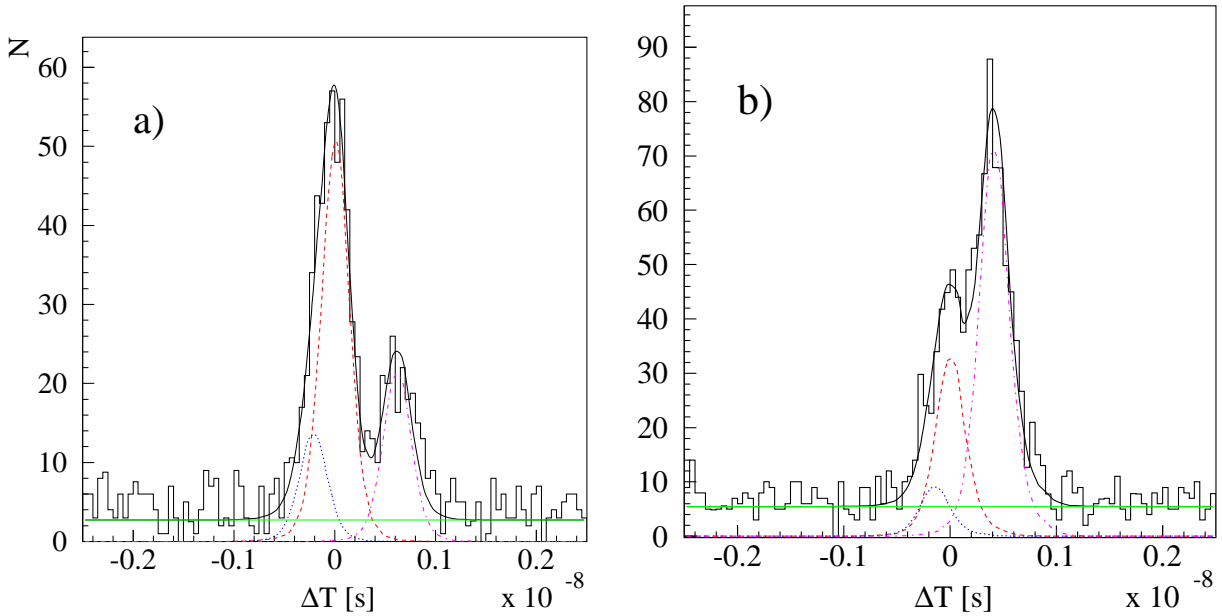


Fig. 4: Distributions over time-of-flight difference for events with positively charged particle momenta in the intervals: a) (4.4–4.5) GeV/c; b) (5.4–5.5) GeV/c. Experimental data (histogram) are fitted by the sum of the distributions: $K^+ \pi^-$ (red, dashed), $\pi^+ \pi^-$ (blue, dotted), $p \pi^-$ (magenta, dotted-dashed) and accidental pairs (green, constant). The sum of all the fractions is shown as black solid line.

the same as for Coulomb pairs. The description of the charged particle propagation through the setup takes into account: a) multiple scattering in the target, detector planes and setup partitions, b) response of all detectors, c) additional momentum smearing and d) results of the SFD response analysis [33, 38, 39] with influence on the Q_T resolution.

6 Data analysis

In the analysis of πK data, the experimental 1-dimensional distributions of relative momentum Q and $|Q_L|$ and the 2-dimensional distributions ($|Q_L|, Q_T$) have been fitted for each year and each πK charge combination by simulated distributions of atomic, Coulomb and non-Coulomb pairs. Their corresponding numbers n_A , N_C and N_{nC} are free fit parameters. The sum of these parameters is equal to the number of analysed events.

The experimental and simulated Q distributions of π^-K^+ and π^+K^- pairs are shown in Fig. 5 (top) for all events with $Q_T < 4$ MeV/c and $|Q_L| < 20$ MeV/c. One observes an excess of events above the sum of Coulomb and non-Coulomb pairs in the low Q region, where atomic pairs are expected. After background subtraction there is a signal at the level of 5.7 standard deviations, shown in Fig. 5 (bottom): $n_A = 349 \pm 61$ ($\chi^2/n = 41/37$, n = number of degrees of freedom), see Table 1. The signal shape is described by the simulated distribution of atomic pairs. The numbers of atomic pairs, produced in the Ni and Pt targets, are $n_A(\text{Ni}) = 275 \pm 57$ ($\chi^2/n = 40/37$) and $n_A(\text{Pt}) = 73 \pm 22$ ($\chi^2/n = 40/36$), respectively. The same analysis has been performed for all π^-K^+ and π^+K^- pairs separately as presented in Fig. 6 and Fig. 7. The π^-K^+ and π^+K^- atomic pair numbers are $n_A = 243 \pm 51$ ($\chi^2/n = 36/37$) and $n_A = 106 \pm 32$ ($\chi^2/n = 42/37$), respectively. The experimental ratio, 2.3 ± 0.9 , between the two types of atom production is compatible with the ratio 2.4 as calculated using FRITIOF [40].

In the 2-dimensional ($|Q_L|, Q_T$) analysis, all experimental data in the same $|Q_L|$ and Q_T intervals have been analysed using simulated 2-dimensional distributions. The evaluated atomic pair number, $n_A = 314 \pm 59$ ($\chi^2/n = 237/157$), corresponds to 5.3 standard deviations and coincides with the previous analysis result.

In Table 1, the results of the three analysis types (Ni and Pt target together) are presented for each atom type and combined. There is a good agreement between the results of the Q and ($|Q_L|, Q_T$) analyses. The 1-dimensional $|Q_L|$ analysis for all πK data yields $n_A = 230 \pm 92$ ($\chi^2/n = 52/37$), which does not contradict the values obtained in the other two statistically more precise analyses.

Compared to the previous investigation [1], in the present work the Pt data has been analysed including upstream detectors. The consequence is a decrease of the statistics, but on the other hand an increase of the Q_T resolution. This better resolution improves the data quality. Concerning the Ni target, the increase of n_A , compared to [3], is caused by optimizing the time-of-flight criteria, which decreases atomic pair losses for the same fraction of background in the final distributions.

Table 1: Atomic pair numbers n_A by analysing the 1-dimensional Q and $|Q_L|$ distributions and the 2-dimensional ($|Q_L|, Q_T$) distribution. Only statistical errors are given.

Analysis	π^-K^+	π^+K^-	π^-K^+ and π^+K^-
Q	243 ± 51 (4.7 σ)	106 ± 32 (3.3 σ)	349 ± 61 (5.7 σ)
$ Q_L $	164 ± 79 (2.1 σ)	67 ± 47 (1.4 σ)	230 ± 92 (2.5 σ)
$ Q_L , Q_T$	237 ± 50 (4.7 σ)	78 ± 32 (2.5 σ)	314 ± 59 (5.3 σ)

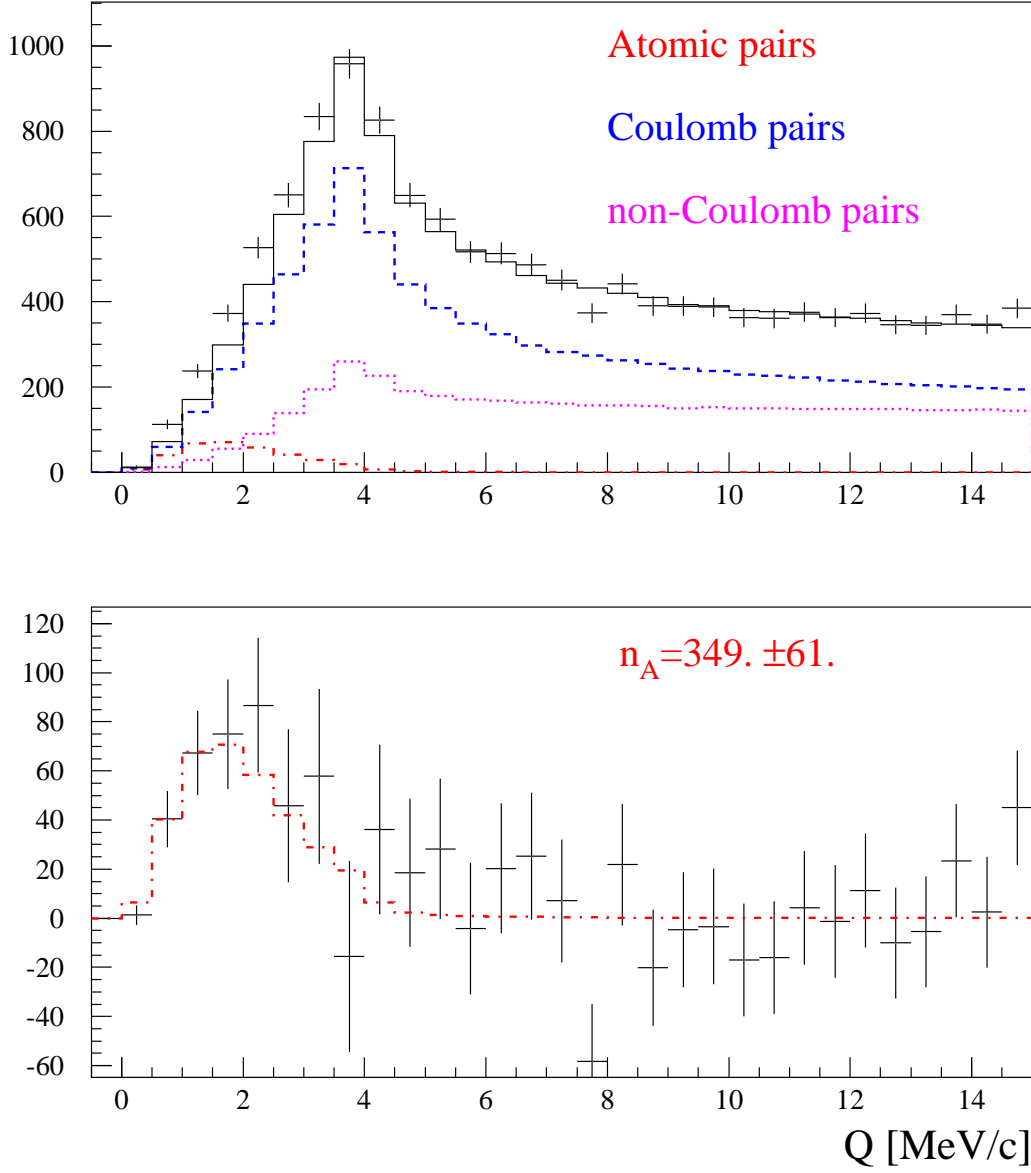


Fig. 5: Top: Q distribution of experimental π^-K^+ and π^+K^- pairs fitted by the sum of simulated distributions of atomic, Coulomb and non-Coulomb pairs. Atomic pairs are shown in red (dotted-dashed) and free pairs (Coulomb in blue (dashed) and non-Coulomb in magenta (dotted)) in black (solid). Bottom: Difference distribution between experimental and simulated free pair distributions compared with simulated atomic pairs. The number of observed atomic pairs is denoted by n_A .

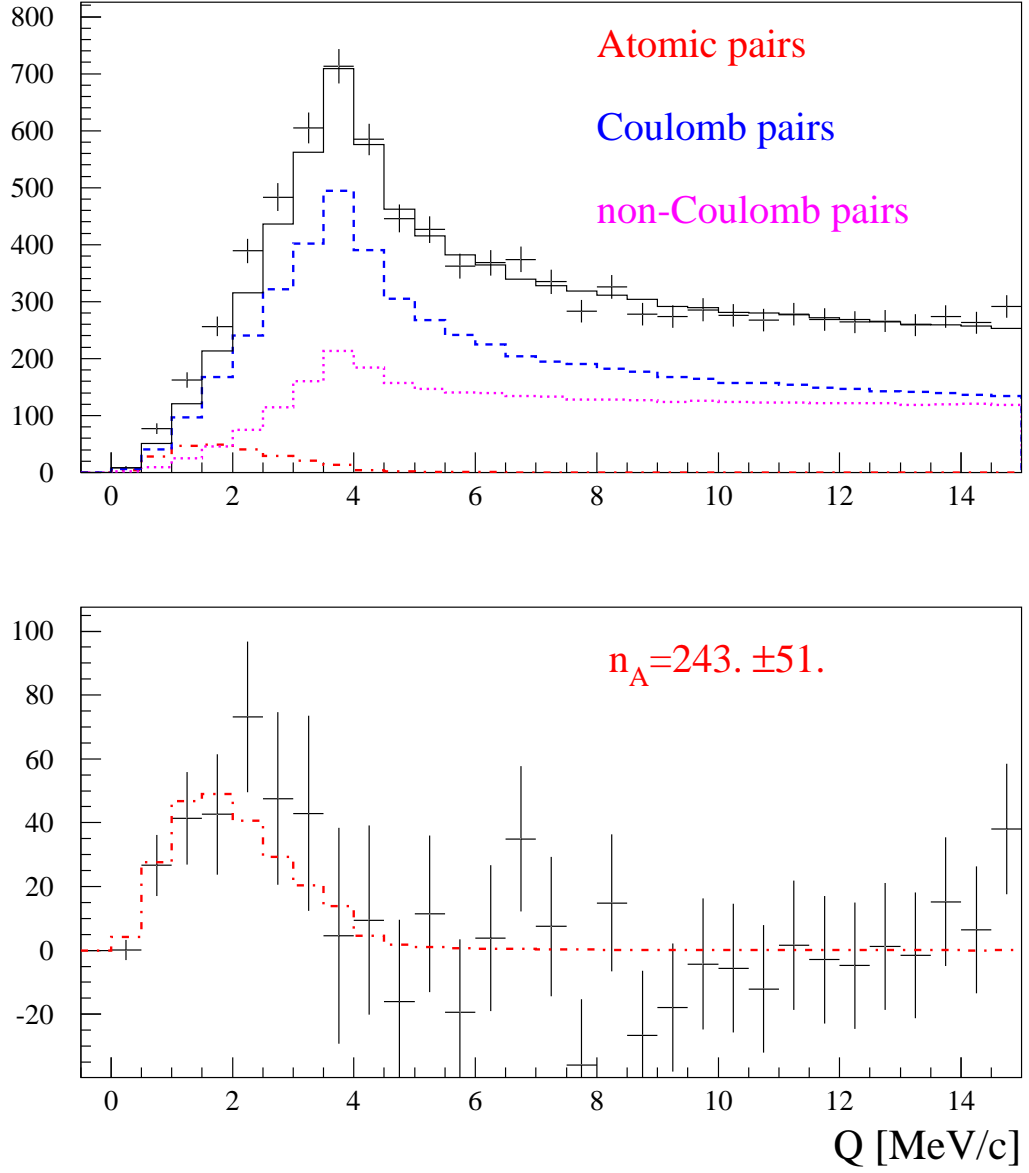


Fig. 6: Same distributions as in Fig. 5, but only for $\pi^- K^+$ pairs.

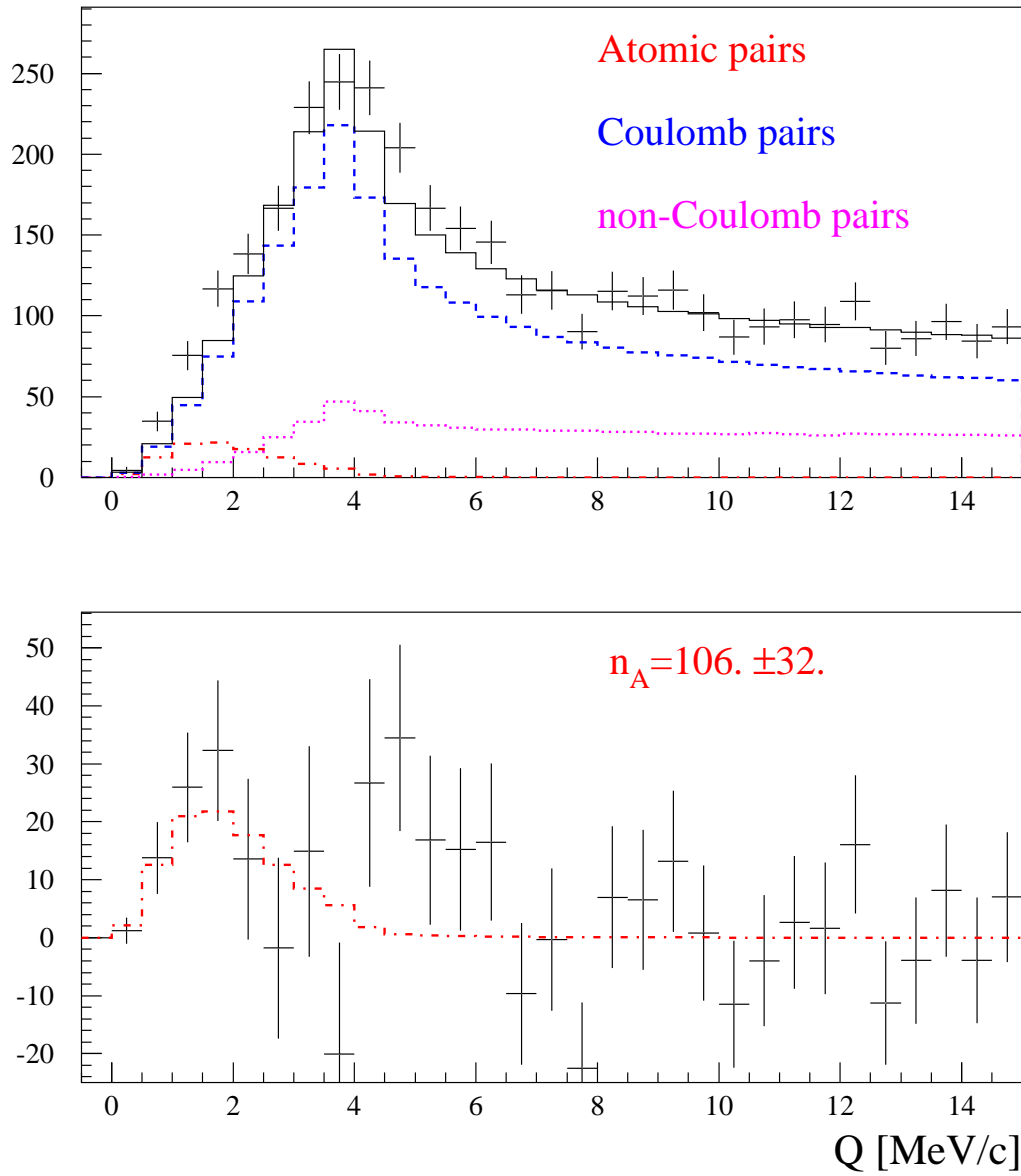


Fig. 7: Same distributions as in Fig. 5, but only for π^+K^- pairs.

7 Systematic errors

The evaluation of the atomic pair number n_A is affected by several sources of systematic errors [29, 33]. Most of them are induced by imperfections in the simulation of the different πK pairs (atomic, Coulomb, non-Coulomb) and misidentified pairs. Shape differences of experimental and simulated distributions in the fit procedure (section 6) lead to biases of parameters, including atomic pair contribution, and finally on n_A . The influence of systematic error sources is different for the analyses of Q , $(|Q_L|, Q_T)$ and Q_L distributions. Table 2 shows systematic errors induced by different sources.

Table 2: Systematic errors in the number n_A of πK atomic pairs.

Sources of systematic errors	σ_Q^{syst}	$\sigma_{Q_L}^{syst}$	$\sigma_{ Q_L , Q_T}^{syst}$
Uncertainty in Λ width correction	0.8	3.0	2.0
Uncertainty of multiple scattering in Ni target	4.4	0.7	2.7
Accuracy of SFD simulation	0.2	0.0	0.1
Correction of Coulomb correlation function on finite size production region	0.0	0.2	0.1
Uncertainty in πK pair laboratory momentum spectrum	3.3	5.4	7.8
Uncertainty in laboratory momentum spectrum of background pairs	6.6	1.6	5.4
Total	8.6	6.4	10.1

8 Conclusion

In the dedicated experiment DIRAC at CERN, the dimesonic Coulomb bound states involving strangeness, π^-K^+ and π^+K^- atoms, have been observed for the first time with reliable statistics. These atoms are generated by a 24 GeV/c proton beam, hitting Pt and Ni targets. In the same targets, a fraction of the produced atoms breaks up, leading to π^-K^+ and π^+K^- atomic pairs with small relative c.m. momenta Q . The 1-dimensional $\pi^\mp K^\pm$ analysis in Q yields $349 \pm 61(stat) \pm 9(syst) = 349 \pm 62(tot)$ atomic pairs (5.6 standard deviations) for both charge combinations. Analogously, a 2-dimensional analysis in $(|Q_L|, Q_T)$ has been performed with the result of $314 \pm 59(stat) \pm 10(syst) = 314 \pm 60(tot)$ atomic pairs (5.2 standard deviations), in agreement with the former number.

The resulting πK atom lifetime and πK scattering length from the ongoing analysis will be presented in a separate paper.

Acknowledgements

We are grateful to R. Steerenberg and the CERN-PS crew for the delivery of a high quality proton beam and the permanent effort to improve the beam characteristics. The project DIRAC has been supported by the CERN and JINR administration, Ministry of Education and Youth of the Czech Republic by project LG130131, the Istituto Nazionale di Fisica Nucleare and the University of Messina (Italy), the

Grant-in-Aid for Scientific Research from the Japan Society for the Promotion of Science, the Ministry of Education and Research (Romania), the Ministry of Education and Science of the Russian Federation and Russian Foundation for Basic Research, the Dirección Xeral de Investigación, Desenvolvemento e Innovación, Xunta de Galicia (Spain) and the Swiss National Science Foundation.

References

- [1] B. Adeva et al., Phys. Lett. B674 (2009) 11.
- [2] Y. Allkofer, PhD thesis, Universität Zürich, 2008.
- [3] B. Adeva et al., Phys. Lett. B735 (2014) 288.
- [4] S. Weinberg, Phys. Rev. Lett. 17 (1966) 616.
- [5] J. Gasser, H. Leutwyler, Nucl. Phys. B250 (1985) 465.
- [6] B. Moussallam, Eur. Phys. J. C14 (2000) 111.
- [7] G. Colangelo, J. Gasser, H. Leutwyler, Nucl. Phys. B603 (2001) 125.
- [8] L. Afanasyev et al., Phys. Lett. B308 (1993) 200.
- [9] B. Adeva et al., Phys. Lett. B619 (2005) 50.
- [10] B. Adeva et al., Phys. Lett. B704 (2011) 24.
- [11] S.M. Bilen'kii et al., Yad. Fiz. 10 (1969) 812; (Sov. J. Nucl. Phys. 10 (1969) 469).
- [12] J. Schweizer, Phys. Lett. B587 (2004) 33.
- [13] V. Bernard, N. Kaiser and U.-G. Meissner, Phys. Rev. D43 (1991) 2757; Nucl. Phys. B357 (1991) 129.
- [14] B. Kubis, U.G. Meissner, Phys. Lett. B529 (2002) 69.
- [15] J. Bijnens, P. Dhonte, P. Talavera, JHEP 0405 (2004) 036.
- [16] P. Buettiker, S. Descotes-Genon, B. Moussallam, Eur. Phys. J. C33 (2004) 409.
- [17] K. Sasaki et al., Phys. Rev. D89 (2014) 054502.
- [18] L. Nemenov, Yad. Fiz. 41 (1985) 980; (Sov. J. Nucl. Phys. 41 (1985) 629).
- [19] B. Adeva et al., CERN-PH-EP-2015-175.
- [20] O. Gorchakov, A. Kuptsov, DN-2005-05, cds.cern.ch/record/1369686.
- [21] O. Gorchakov, DN-2005-23, cds.cern.ch/record/1369668.
- [22] A. Sommerfeld, Atombau und Spektrallinien, F. Vieweg Sohn (1931).
- [23] G. Gamov, Z. Phys. 51 (1928) 204.
- [24] A. Sakharov, Zh. Eksp. Teor. Fiz. 18 (1948) 631; Sov. Phys. Usp. 34 (1991) 375.
- [25] L. Afanasyev, O. Voskresenskaya, Phys. Lett. B453 (1999) 302.
- [26] R. Lednicky, J. Phys. G: Nucl. Part. Phys. 35 (2008) 125109.
- [27] A. Benelli, V. Yazkov, DN-2013-03, cds.cern.ch/record/1622175.
- [28] O. Gortchakov, DN-2009-10, 2009-02, cds.cern.ch/record/1369625, 1369633.
- [29] A. Benelli, V. Yazkov, DN-2016-01, cds.cern.ch/record/2137645.
- [30] J. Beringer et al. (Particle Data Group), Phys. Rev. D86 (2012) 010001.
- [31] P. Doskarova, V. Yazkov, DN-2013-05, cds.cern.ch/record/1628541.
- [32] A. Benelli, V. Yazkov, DN-2009-07, cds.cern.ch/record/1369628.
- [33] V. Yazkov, M. Zhabitsky, DN-2013-06, cds.cern.ch/record/1628544.
- [34] M.V. Zhabitsky, DN-2007-11, cds.cern.ch/record/1369651.
- [35] O. Gorchakov, DN-2010-01, cds.cern.ch/record/1369624.
- [36] M. Zhabitsky, Phys. At. Nucl. 71 (2008) 1040.

- [37] L. Afanasyev, A. Tarasov, Phys. At. Nucl. 59 (1996) 2130.
- [38] A. Gorin et al., Nucl. Instrum. Meth. A566 (2006) 500.
- [39] A. Benelli, SFD study and simulation for the data 2008-2010, DIRAC-TALK-2011-01.
- [40] O. Gorchakov, L. Nemenov, DN-2015-05 (DN=DIRAC-NOTE), cds.cern.ch/record/2120667.